Incorporating Sharp Features in the General Solid Sweep Framework

Bharat Adsul[1], Jinesh Machchhar[1], Milind Sohoni[1]

[1] Department of Computer Science and Engineering, Indian Institute of Technology Bombay, India

Abstract

This paper extends a recently proposed robust computational framework for constructing the boundary representation (brep) of the volume swept by a given smooth solid moving along a one parameter family h of rigid motions. Our extension allows the input solid to have sharp features, and thus it is a significant and useful generalization of that work.

This naturally requires a precise description of the geometry of the surface generated by the sweep of a sharp edge supported by two intersecting smooth faces. We uncover the geometry along with the related issues like parametrization and singularities via a novel mathematical analysis. Correct trimming of such a surface is achieved by an analysis of the interplay between the cone of normals at a sharp point and its trajectory under h. The overall topology is explained by a key lifting theorem which allows us to compute the adjacency relations amongst entities in the swept volume by relating them to corresponding adjacencies in the input solid. Moreover, global issues related to body-check such as orientation and singularities are efficiently resolved. Many examples from a pilot implementation illustrate the efficiency and effectiveness of our framework.

1 Introduction

In this paper we investigate the computation of the swept volume of a given solid moving along a smooth one parameter family of rigid motions. We assume the solid to be of class G0, wherein, the unit outward normal may be discontinuous at the intersection of two or more faces. An example of solid sweep appears in Figure 1. Sweeping has several applications, viz. CNC-machining verification [12, 13], collision detection, motion planning [1] and packaging [11].

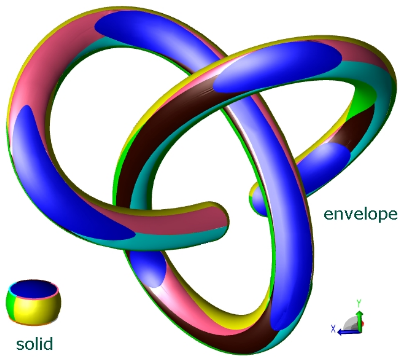

Figure 1: An example of swept volume.

We adopt the industry standard parametric boundary representation (brep) format to input the solid and output the swept volume. In the brep format, the solid M is represented by its boundary ∂M which separates the interior of M from its exterior. The brep of M consists of the parametric definitions of the faces, edges and vertices as well as their orientations and adjacency relations amongst these. Figure 2(a) schematically illustrates such a solid.

In this paper we extend the framework proposed in [4] to input solids of class G0. This is done by extending the key constructs of the *funnel* and the *correspondence* from the smooth faces of ∂M to the sharp features of ∂M. This, along with the topology and geometry generated by smooth faces of ∂M outlined in [4] and the trimming of self-intersections described in [3] gives a complete framework for computing the brep of the general swept volume.

An edge or a vertex of ∂M is called **sharp** if it (or its part) lies in the intersection of faces meeting with G1-discontinuity. For instance, in the solid shown in Figure 2(a), the faces F_1 and F_2 meet in the sharp edge E_1 while faces F_2 and F_3 meet smoothly in edge E_2. The partner co-edges c_1 and c_1' for E_1 associated with faces F_1 and F_2 respectively and a sharp vertex Z_1 are also shown. In this work we focus on the entities in the brep of envelope $\mathcal{E}$ which are generated by sharp edges and vertices of ∂M. This involves the following considerations.

1. Geometry: The local geometry of the entity $\mathcal{E}^E$ in the brep of $\mathcal{E}$ generated by a sharp edge $E \subset \partial M$ can be modeled by that of the 'free' edge E moving in $\mathbb{R}^3$. The surface S^E swept by such an edge is smooth except when the velocity at a point is tangent to the edge at that point.
2. Trim: In order to obtain $\mathcal{E}^E$, S^E needs to be suitably trimmed. The correct trimming follows as a result of the interplay between the cone of normals at a sharp point and the trajectory of the point under the family of rigid motions. In the schematic shown in Figure 2, an object with sharp features undergoes translation with compounded rotation indicated with dotted arrows. In the positions shown in Figure 2(b) and Figure 2(d), the sharp feature does not generate any points on the envelope while in Figure 2(c) it does.
3. Orientation: The faces $\mathcal{E}^E$ must be oriented so that the unit normal at each point of $\mathcal{E}^E$ points in the exterior of the swept volume $\mathcal{V}$.

We now outline the structure of this paper. In Section 2, we compare our contributions with previous related work. In Section 3, we elaborate on the mathematics of the envelope. We establish a natural correspondence π between the boundary of

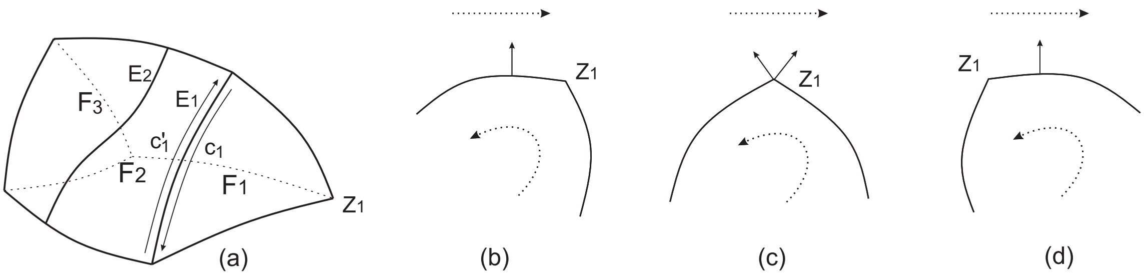

Figure 2: Geometry generated by sharp features.

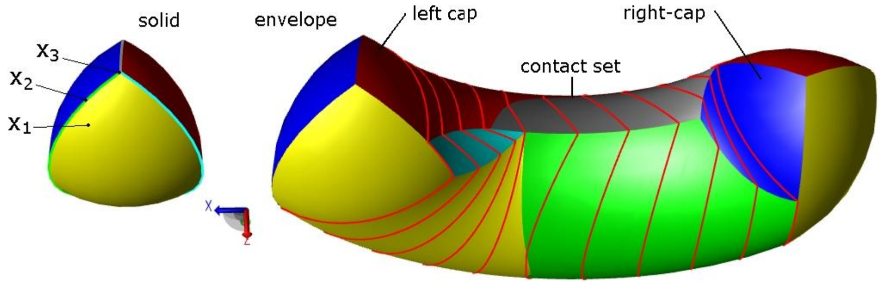

Figure 3: A solid undergoing translation along a circular arc in xy-plane and rotation about y-axis. Curves of contact at few time instants are shown on the envelope in red.

the input solid and the boundary of the swept volume which serves as a basis for a brep structure on $\mathcal{E}$. In Section 4 we give the overall solid sweep framework and outline how it extends the framework proposed in [4] to handle sharp features of ∂M. The faces and edges of $\mathcal{E}$ generated by sharp features of ∂M are parametrized in Section 5. This is followed by the analysis of the adjacency relations amongst the entities of $\mathcal{E}$ via the correspondence map π and is explained in Section 6. We show that there is local similarity between the brep structure of $\mathcal{E}$ and that of ∂M. In Section 7 we explain the steps of the overall computational framework given in Section 4. We give many sweep examples demonstrating the effectiveness of our algorithm. In Section 8, we discuss subtle issues of self-intersections and how they can be handled. Finally, we conclude in Section 9 with remarks on extension of this work.

2 Related work

The computation of swept volume has been extensively studied [2, 5, 7, 8, 9, 10, 14, 17]. Abdel-Malek et al. [2], model the envelope as solution set of the Jacobian rank deficiency condition. This approach relies on symbolic computation and does not accept free form surfaces as input. Blackmore et al. [5] derive a differential equation whose solution is the envelope. This method does not meet the tolerance requirements of modern kernels. Erdim et al. [8] give a point membership test for a point to belong inside, outside or on the boundary of the swept volume. This yields a parametric implicit representation of the envelope whose conversion to brep may be computationally expensive. The solid-sweep framework of Adsul et al. [4] offers a mathematical analysis which extends both the geometric as well as the topological understanding of the solid sweep. This is done by a deeper analysis of parametrization, self-intersection and the interaction of faces, edges and vertices of a smooth solid in brep format.

Two works which need separate mention are [14] and [12]. Martin et al. [14] offer a conceptual framework for the solid sweep which is closest to ours but does not completely analyse the issues of parametrization, singularities, local self-intersection and orientation. Lee et al. [12] consider the sweep of an axially symmetric tool and do consider a tool which has sharp edges. However, for them, the sweep is represented by imprinting the contact curves on the tool itself. Thus, the general situation and trimming are not considered. Our notion of the cone bundle provides for this.

3 Mathematical structure of the general sweep

This section extends to sharp solids, two key constructions, viz., (i) the definition of the envelope, and (ii) the natural brep structure.

Definition 1. *A* **trajectory** *in* $\mathbb{R}^3$ *is specified by a map*

$$h : I \to (SO(3), \mathbb{R}^3), h(t) = (A(t), b(t))$$

where I *is a closed interval of* $\mathbb{R}$, $A(t) \in SO(3)$[1], $b(t) \in \mathbb{R}^3$. *The parameter* t *represents time.*

Assumption 2. *We make the following key assumption about* (M, h). *The tuple* (M, h) *is in a* general position. *The motion* h *is of class* C^k *for some* $k \geq 2$, *i.e., partial derivatives of order up to* k *exist and are continuous.*

The above assumption about the general position of (M, h) is equivalent to requiring that slight perturbation of M or h does not change the topology of the brep structure of the swept volume.

Definition 3. *The* **action** *of* h *(at time* t *in* I*) on* M *is given by* $M(t) = \{A(t) \cdot x + b(t) | x \in M\}$. *The* **swept volume** $\mathcal{V}$ *is the union* $\bigcup_{t \in I} M(t)$ *and the* **envelope** $\mathcal{E}$ *is defined as the boundary of the swept volume* $\mathcal{V}$.

An example of a swept volume appears in Figure 3. Clearly, for each point y of $\mathcal{E}$ there must be an $x \in M$ and a $t \in I$ such that $y = A(t) \cdot x + b(t)$.

We denote the interior of a set W by W^o and its boundary by ∂W. It is clear that $\mathcal{V}^o = \cup_{t \in I} M(t)^o$. Therefore, if $x \in M^o$, then for all $t \in I$, $A(t) \cdot x + b(t) \notin \mathcal{E}$. Thus, the points in the interior of M do not contribute any point on the envelope.

[1] $SO(3) = \{X$ is a 3 ×3 real matrix$|X^t \cdot X = I, det(X) = 1\}$ is the special orthogonal group, i.e. the group of rotational transforms.

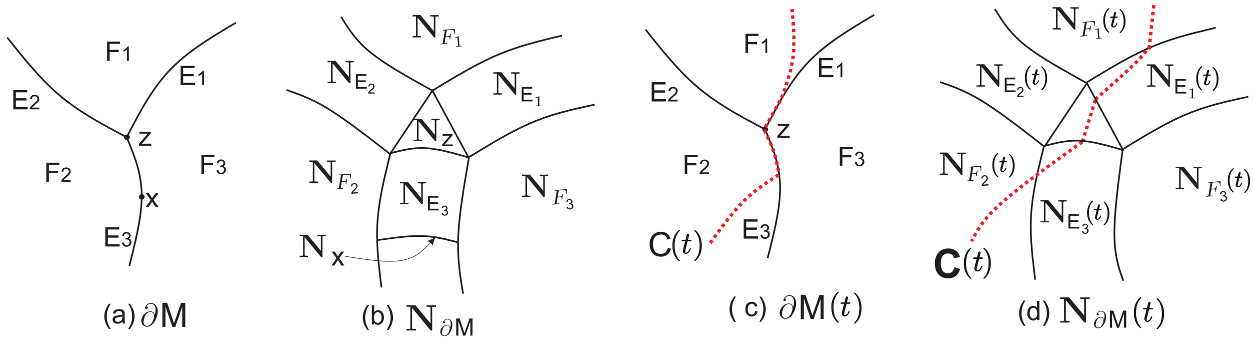

Figure 4: (a) Solid boundary ∂M (b) Unit normal bundle for ∂M (c) $C(t)$ (d) $\mathbf{C}(t)$

Definition 4. *For a point $x \in M$, define the* **trajectory of x** *as the map $\gamma_x : I \to \mathbb{R}^3$ given by $\gamma_x(t) = A(t) \cdot x + b(t)$ and the velocity $v_x(t)$ as $v_x(t) = \gamma'_x(t) = A'(t) \cdot x + b'(t)$.*

We now recall the fundamental proposition from [4, 5] and also elsewhere which provides a necessary condition for a point $x \in \partial M$ to contribute the point $\gamma_x(t)$ on $\mathcal{E}$ at time t, assuming that M is *smooth*. Let N_x denote the unique unit outward normal to ∂M at $x \in \partial M$.

Proposition 5. *Define the function $G : \partial M \times I \to \mathbb{R}$ as $G(x,t) = \langle A(t) \cdot N_x, v_x(t) \rangle$. Let $I = [t_0, t_1], t \in I$ and $x \in \partial M$ be such that $\gamma_x(t) \in \mathcal{E}$. Then either (i) $t = t_0$ and $G(x,t) \leq 0$, or (ii) $t = t_1$ and $G(x,t) \geq 0$, or (iii) $G(x,t) = 0$.*

Now we develop some notation in order to generalize the above proposition to non-smooth M represented in the brep format. Recall that the brep of M models ∂M through a collection of faces which meet each other across edges which in turn meet at vertices. Clearly, the sharp features of M are located along the edges and vertices.

The solid M may be (partly) convex/concave at a sharp edge. For the moment we only consider solids that do not have concave edges. See Section 8 for a discussion on concave edges. Further, for simplicity, we assume that at most three faces meet at a sharp vertex in ∂M. Thus, in the following definition, m is either $1, 2$ or 3.

Definition 6. *For a point $x \in \bigcap_{i=1}^{m} F_i$, define the* **cone of unit outward normals** *to ∂M at x as the intersection of the unit sphere S^2 with the convex cone formed by N_i, for $i = 1, \ldots, m$, where N_i is the unit outward normal to F_i at x. For simplicity, we assume that N_i for $i = 1, \ldots, m$ are linearly independent. We denote the cone of unit normals at x by N_x.*

The points labeled x_3 and x_2 in Figure 3 lie in the intersection of three and two smooth faces respectively meeting sharply. The point labeled x_1 lies in the interior of a smooth face, hence N_{x_1} has a single element, namely, outward normal to ∂M at x_1. The cone of normals at a point is referred to as the *extended Tool map* in [12].

Definition 7. *For a subset X of ∂M, the* **unit normal bundle** *(associated to X) is defined as the disjoint union of the cones of unit normals at each point in X and denoted by $\mathbf{N_X}$, i.e., $\mathbf{N_X} = \bigsqcup_{x \in X} N_x = \bigcup_{x \in X} \{(x, n) | n \in N_x\}$.*

In Figure 4(a) a portion of ∂M is shown in which three faces F_i and three edges E_i meet at a sharp vertex Z. Note that for $X \subset \partial M$, $\mathbf{N_X} \subset \mathbb{R}^3 \times S^2$, where S^2 is the unit sphere in $\mathbb{R}^3$. However, for the ease of illustration we have shown the unit normal bundles $\mathbf{N_{F_i}}, \mathbf{N_{E_i}}$ for $i = 1, 2, 3$ and $\mathbf{N_Z}$ schematically in Figure 4(b) in which an element $(x, n) \in \mathbf{N_{\partial M}}$ is represented as the point $x + n$.

We now state the following important proposition whose proof is straight-forward.

Proposition 8. *The bundle $\mathbf{N_{\partial M}}$ is a piece-wise smooth and continuous manifold. There is a natural projection $\mu : \mathbf{N_{\partial M}} \to \partial M$ given by $\mu(x, n) = x$ which is continuous.*

For $x \in \partial M$ and $t \in I$, the cone of unit normals to $\partial M(t)$ at the point $\gamma_x(t)$ is given by $A(t) \cdot N_x := \{A(t) \cdot n | n \in N_x\}$. Further, the action of h at time $t \in I$ on the unit normal bundle $\mathbf{N_{\partial M}}$ is given by $\mathbf{N_{\partial M}}(t) := \{(\gamma_x(t), A(t) \cdot n) | x \in \partial M, n \in N_x\}$. The projection from $\mathbf{N_{\partial M}}(t)$ to $\partial M(t)$ given by $(\gamma_x(t), A(t) \cdot n) \mapsto \gamma_x(t)$ will be denoted again by μ.

Definition 9. *For $(x, n) \in \mathbf{N_{\partial M}}$ and $t \in I$, define the function $g : \mathbf{N_{\partial M}} \times I \to \mathbb{R}$ as $g(x, n, t) = \langle A(t) \cdot n, v_x(t) \rangle$.*

Thus, $g(x, n, t)$ is the dot product of the velocity with the normal $A(t) \cdot n \in A(t) \cdot N_x$ at the point $\gamma_x(t) \in \partial M(t)$. We are now ready to state the next Proposition which naturally generalizes Proposition 5 to non-smooth solids.

Proposition 10. *Let $I = [t_0, t_1], t \in I$ and $x \in \partial M$ be such that $\gamma_x(t) \in \mathcal{E}$. Then either (i) $t = t_0$ and there exists $n \in N_x$ such that $g(x, n, t) \leq 0$ or (ii) $t = t_1$ and there exists $n \in N_x$ such that $g(x, n, t) \geq 0$ or (iii) there exists $n \in N_x$ such that $g(x, n, t) = 0$.*

Refer to the appendix for proof.

Definition 11. *Fix a time instant $t \in I$. The set $\{\gamma_x(t) \in \partial M(t) | \exists n \in N_x$ such that $g(x, n, t) = 0\}$ is referred to as the* **curve of contact** *at t and denoted by $C(t)$. The set $\{(\gamma_x(t), A(t) \cdot n) \in \mathbf{N_{\partial M}}(t) | g(x, n, t) = 0\}$ is referred to as the* **normals of contact at** *t and denoted by $\mathbf{C}(t)$. Further, the union of curves of contact is referred to as the* **contact set** *and denoted by C, i.e., $C = \bigcup_{t \in I} C(t)$. The union $\bigcup_{t \in I} \mathbf{C}(t)$ is referred to as the* **normals of contact** *and denoted by $\mathbf{C}$.*

Proposition 10 is tantamount to saying that $\mu(\mathbf{C(t)}) = C(t)$. Curves of contact at a few time instants are shown in the sweep example of Figure 3 in red. Figures 4(c) and 4(d) schematically illustrate the curve of contact and the normals of contact at a time instant t, shown as dotted curves in red. The curve of contact is referred to as the characteristic curve in [15]. The normals of contact at t are referred to as the contact map in [12].

The **left cap** is defined as $L_{cap} = \{\gamma_x(t_0) \in \partial M(t_0) | \exists n \in N_x$ such that $g(x, n, t_0) \leq 0\}$ and the **right cap** is defined as $R_{cap} = \{\gamma_x(t_1) \in \partial M(t_1) | \exists n \in N_x$ such that $g(x, n, t_1) \geq 0\}$. The left cap and right cap are shown in the sweep example of Figure 3. The left and right caps are easily computed from the solid at initial and final positions.

Note that, by Proposition 10, $\mathcal{E} \subseteq L_{cap} \cup C \cup R_{cap}$. In general, a point on the contact set C may not appear on the complete envelope $\mathcal{E}$ as it may get occluded by an interior point of the solid at a different time instant. This complicates the correct construction of the envelope by an appropriate *trimming* of the contact-set. We refer the reader to [3] for a comprehensive mathematical analysis of the trimming and related issues arising due to local/global self-intersections of the family $\{C(t)\}_{t \in I}$. We will largely stick to the case of *simple* sweeps for clarity. Non-simple sweeps are discussed in Section 8.

Definition 12. *A sweep (M, h) is said to be simple if the envelope is the union of the contact set, the left cap and the right cap, i.e., $\mathcal{E} = L_{cap} \cup C \cup R_{cap}$.*

Hence, in a simple sweep, every point on the contact set appears on the envelope and no trimming of the contact set is required in order to obtain the envelope.

Lemma 13. *For a simple sweep, for $t \neq t'$, $C(t) \cap C(t') = \emptyset$. In short, no two distinct curves of contact intersect.*

Refer to [4] for proof.

Definition 14. *For a simple sweep, define the natural correspondence $\pi : C \to \partial M$ as follows: for $y \in C(t)$, we set $\pi(y) = x$ where x is the unique point on ∂M such that $\gamma_x(t) = y$.*

Thanks to Lemma 13, π is well-defined. Thus, $\pi(y)$ is the natural point on ∂M which transforms to y through the sweeping process.

The correspondence π induces a natural brep structure on $\mathcal{E}$ which is derived from that of ∂M. The map π is illustrated via color coding in the sweep examples shown in Figures 1, 3 and 12 by showing the points y and $\pi(y)$ in the same color.

A face of ∂M generates a set of faces on the contact set C. An edge or a vertex where ∂M is G1-continuous generates a set of edges or vertices respectively on C. However, a sharp edge of ∂M generates a set of faces on C and a sharp vertex generates a set of edges on C. This is illustrated in the example of Figure 1 by the sharp edge shown in pink which generates faces on C shown in pink. For $O \subseteq \partial M$, we denote the contact set generated by O by C^O, i.e., $C^O = \{y \in C | \pi(y) \in O\}$. Note that while O is connected, the corresponding contact set C^O may not be. A connected component of C^O is denoted using a subscript, for example, faces C_1^E, C_2^E and so on.

4 The computational framework

Algorithm 1 given below is an extension of that in [4] to the case of sharp edges. The key steps are from step 14.

Algorithm 1 Solid sweep

1: **for all** faces F in ∂M **do**
2:     **for all** co-edges c in ∂F **do**
3:         **for all** z in ∂c **do**
4:             Compute vertices C^z generated by z
5:         **end for**
6:         Compute co-edges C^c generated by c
7:         Orient co-edges C^c
8:     **end for**
9:     Compute $C^F(t_0)$ and $C^F(t_1)$
10:     Compute loops bounding faces C^F which will be generated by F
11:     Compute faces C^F generated by F
12:     Orient faces C^F
13: **end for**
14: **for all** sharp edges E in ∂M **do**
15:     **for all** Z in ∂E **do**
16:         Compute co-edges C^Z generated by Z
17:         Orient co-edges C^Z
18:     **end for**
19:     $(F, F') \leftarrow AdjacentFaces(E)$
20:     Compute co-edges $C^E \cap C^F$ and $C^E \cap C^{F'}$
21:     Orient co-edges $C^E \cap C^F$ and $C^E \cap C^{F'}$
22:     Compute $C^E(t_0)$ and $C^E(t_1)$
23:     Compute loops bounding faces C^E which will be generated by E
24:     Compute faces C^E generated by E
25:     Orient faces C^E
26: **end for**
27: Compute adjacencies between faces of C

We outline what was achieved in [4]. At the heart of Algorithm 1 is an entity-wise *implementation* of the correspondence π which is a classification of the faces, edges and vertices of $\mathcal{E}$ by the generating entity in ∂M. This is achieved by computing C^O of the envelope for key entities $O \subseteq \partial M$ which yield faces in $\mathcal{E}$. The smooth case is topologically simple since faces generate faces, edges generate edges and so on. The computation of C^O is followed by an orientation calculation. It was noted that while the adjacencies of entities in $\mathcal{E}$ were built from that on ∂M, the orientation on $\mathcal{E}$ was *not* as on ∂M and in fact could be positive, negative or zero *vis a vis* that on ∂M.

At the end of step 13, it is assumed that for each smooth face/edge F of ∂M, its contribution to the envelope $\mathcal{E}$ is available as a brep face/edge. The issue now is to generate the entities which arise from sharp edges and vertices, orient these correctly and *stitch* these together to to construct the final envelope $\mathcal{E}$.

Firstly, note that a sharp vertex generates a set of edges. Steps 15-18 compute the structure of these edges in two steps, viz., computing the geometry and then its orientation. This is explained in Section 5.4. Next, note that a sharp edge E generates a collection of *faces*. The boundary of these faces is computed in steps 19-23. The geometry and the detection of singularities is done in step 24 and discussed in Section 5.2 and Section 5.3 respectively. The orientation of faces is achieved in step 25 and discussed in Section 7.4. Finally, step 27 stitches the body from its entities. This is described in Section 6.

The key technical contributions thus are essentially (i) a complete analysis of the geometry, trim curves and orientation of the faces and edges generated by sharp entities, and (ii) a seamless architectural integration of sharp features into the general solid sweep framework.

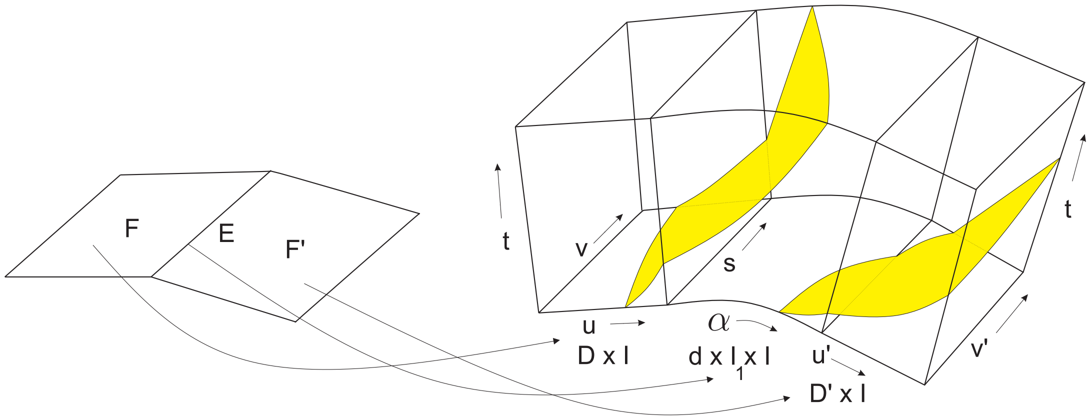

Figure 5: Prisms for faces F, F' and edge E shown adjacent to each other. The funnels of F, F' and pre-funnel of E are shaded in yellow.

An obvious question is why it could not have been done before, i.e., in [4] itself. The answer is of course that the structure of sweeps C^F of smooth faces is the key construct and the C^E, i.e., sweeps of sharp edges are essentially *transition faces*. The theory of these transition faces must interface with that of the smooth faces and was built subsequently.

5 Parametrization and Geometry of faces and edges of C

In this section we describe the parametrization and geometry of the faces and edges of C. We extend the key constructs of *prism* and *funnel* proposed in [4] for smooth faces of ∂M to the sharp features of ∂M. The funnel serves as the parameter space for faces of C^E and guides further computation of the envelope.

Recall that a (smooth and non-degenerate) face is a map $S : D \to \mathbb{R}^3$, where $D \subseteq \mathbb{R}^2$ is a domain bounded by trim curves. A **smooth parametric curve** in $\mathbb{R}^3$ is a (smooth and non-degenerate) map $e : d \to \mathbb{R}^3$ where $d = [s_0, s_1]$ is a closed interval of $\mathbb{R}$. Thus, specifying a face (resp. edge) requires us to specify the functions S (resp. e) and the domain D (resp. d).

5.1 Parametrization of faces C^F

We first recall from [3] the computation of faces C^F generated by a smooth face $F \subseteq \partial M$. Suppose that F is given by the parametrization $S : D \to \mathbb{R}^3$, where D is a domain in $\mathbb{R}^2$ with parameters (u, v). Let I be the interval used to parametrize the motion h. The envelope condition in Proposition 5 yields a function $f^F(u, v, t)$ on the *prism* $D \times I$, viz., $f^F(u, v, t) = \langle A(t) \cdot N(u, v), \gamma'_{S(u,v)}(t)\rangle$ where $N(u, v)$ is the outward normal to F at $S(u, v)$. For simple sweeps $f^F(u, v, t) = 0$ indicates that $A(t) \cdot S(u, v) + b(t)$ is on the envelope. This led to the definition of the funnel $\mathcal{F}^F$ as the zero-set of f^F within the prism. If $\mathcal{F}^F_1, \ldots, \mathcal{F}^F_k$ are the connected components of the funnel then (i) the face F leads to exactly k disjoint faces $C^F_1, \ldots, C^F_k$ in the envelope $\mathcal{E}$, (ii) each $\mathcal{F}^F_i$ serves as the parameter space to implement C^F_i, (iii) the boundary of $\mathcal{F}^F_i$ arises from $\mathcal{F}^F$ intersecting the boundary of the prism and parametrizes the co-edges of C^F_i.

5.2 Parametrization of faces C^E

Let E be a sharp edge of ∂M supported by two faces F and F'. Let e be the curve underlying the sharp edge E and d be the domain of E, i.e., $e(d) = E$. We extend the notion of *prism* proposed in [4] for smooth faces of ∂M to the edge E. At every point $e(s) \in E$, we may parametrize the cone of unit normals $N_{e(s)}$ as $N_{e(s)}(\alpha) = \frac{\alpha \cdot N_1 + (1-\alpha) \cdot N_2}{\|\alpha \cdot N_1 + (1-\alpha) \cdot N_2\|}$ for $\alpha \in I_1 = [0, 1]$, where, N_1 and N_2 are the unit outward normals to F and F' respectively at point $e(s)$. We refer to the subset $d \times I_1 \times I$ of $\mathbb{R}^3$ as the prism of E. A point (s, α, t) in the prism corresponds to the normal $A(t) \cdot N_{e(s)}(\alpha)$ at the point $\gamma_{e(s)}(t)$ in the unit normal bundle $\mathbf{N_E}(t)$. Define the real-valued function f^E on the prism of E as $f^E(s, \alpha, t) = g(e(s), N_{e(s)}(\alpha), t)$. Clearly if $f^E(s, \alpha, t) = 0$ then $\gamma_{e(s)}(t) \in C^E$. We will refer to the zero set of f^E as the **pre-funnel**. See Figure 5 for an illustration of how funnels of smooth faces interact with the pre-funnel of the sharp edge.

Fix a point $x = e(s) \in E$. From Proposition 10 it is easy to see that if $\gamma_x(t) \in C^E$ then either (i) there is a unique $\alpha \in I_1$ such that $f^E(s, \alpha, t) = 0$ or (ii) for all $\alpha \in I_1$, $f^E(s, \alpha, t) = 0$. The later case leads to singularity in C^E and is described in Section 5.3. The former case allows us to eliminate α and define the funnel as the *projection* of the zero-set of f^E above to $d \times I$, as follows:

Definition 15. *For a sweep interval I and a sharp edge $E \subset \partial M$, define $\mathcal{F}^E = \{(s, t) \in d \times I | f^E(s, \alpha, t) = 0$ for some $\alpha \in I_1\}$. The set $\mathcal{F}^E$ is referred to as the* **funnel** *for E. The set $\{(s, t) \in \mathcal{F}^E | t = t'\}$ is referred to as the* **p-curve of contact** *at t' and denoted by $\mathcal{F}^E(t')$.*

The set $\mathcal{F}^E$ serves as the domain of parametrization for the faces C^E generated by E. The parametrization function is given by $\sigma^E : \mathcal{F}^E \to \mathbb{R}^3$ as $\sigma^E(s, t) = A(t) \cdot e(s) + b(t)$.

It now remains to compute the trim curves of $\mathcal{F}^E$. The zero-set of f^E is bounded by the boundaries of the prism $d \times I_1 \times I$. Thus the boundaries of $\mathcal{F}^E$ come from the equations $s = s_0, s_1$ or $t = t_0, t_1$ or finally $\alpha = 0, 1$. The first two conditions are easily implemented. The condition $\alpha = 0$ is equivalent to the assertion that $a^E_1(s, t) = \langle A(t) \cdot N_1(e(s)), \gamma'_{e(s)}(t)\rangle = 0$, where $N_1(e(s))$ is the normal to the face F at the point $e(s)$. The function $a^E_1(s, t) = 0$ and the similarly defined $a^E_2(s, t) = 0$ (for face F') serve as the final trim curves. This collection of trim curves may yield several components, each corresponding to a unique face of C^E on $\mathcal{E}$.

Figure 6(a) illustrates the funnel $\mathcal{F}^E$ shaded in yellow and p-curves of contact $\mathcal{F}^E(t'), \mathcal{F}^E(t'')$ and $\mathcal{F}^E(t''')$ shown in red. In this example, $\mathcal{F}^E$ has two connected components. The curves $\sigma^E(\mathcal{F}^E(t))$ are parts of the curve of contact on $\mathcal{E}$ at time t. In Figure 6(b), the normals of contact, i.e., $A(t) \cdot e'(s) \times \gamma'_x(t)$ at times t', t'' and t''' are shown projected on the unit normal bundle $\mathbf{N_E}$.

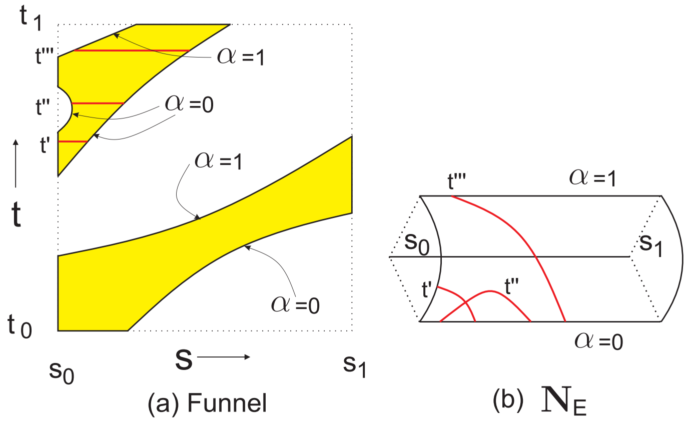

Figure 6: (a) The funnel $\mathcal{F}^E$ is shaded in yellow. The p-curves of contact at t', t'' and t''' are shown in red. (b) The normals of contact at times t', t'' and t'', i.e., $\mathbf{C}(t'), \mathbf{C}(t'')$ and $\mathbf{C}(t''')$ respectively, projected on $\mathbf{N_E}$.

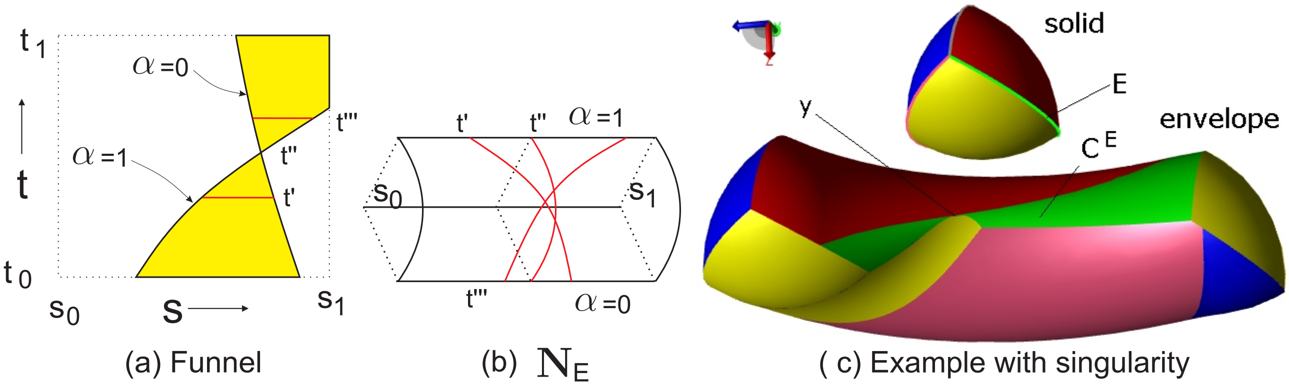

Figure 7: Singularity in C^E. (a) The funnel is shaded in yellow. The p-curves of contact $\mathcal{F}^E(t'), \mathcal{F}^E(t'')$ and $\mathcal{F}^E(t''')$ are shown in red. (b) The normals of contact at times t', t'' and t'', i.e., $\mathbf{C}(t'), \mathbf{C}(t'')$ and $\mathbf{C}(t''')$ respectively, projected on $\mathbf{N_E}$. (c) The contact set C^E has a singularity at point y.

5.3 Singularities in C^E

A parametric surface S is said to have a singularity at a point $S(u_0, v_0)$ if S fails to be an immersion at (u_0, v_0), i.e., the rank of the Jacobian J_S falls below 2.

Lemma 16. *Let $p = (s', t') \in \mathcal{F}^E$. A face of C^E has a singularity at point $\sigma^E(p)$ if and only if the velocity $\gamma'_{e(s')}(t')$ is tangent to the edge E at the point $\sigma^E(p)$, i.e., $\gamma'_{e(s')}(t')$ and $A(t') \cdot \frac{de}{ds}(s')$ are linearly dependent.*

Figure 7(a) illustrates schematically a funnel $\mathcal{F}^E$ having a singularity at time t''. The normals of contact at a few time instants are shown projected on $\mathbf{N_E}$ in red in Figure 7(b). A sweep example with singularity is shown in Figure 7(c).

5.4 Parametrization of edges C^Z

Let Z be a sharp vertex lying in the intersection of faces F_1, F_2 and F_3 and let N_1, N_2 and N_3 be the unit outward normals to F_1, F_2 and F_3 respectively at Z. An element $n \in N_Z$ can be represented as $\frac{\sum_{i=1}^{3} \alpha_i \cdot N_i}{\|\sum_{i=1}^{3} \alpha_i \cdot N_i\|}$ where $\alpha_i \in \mathbb{R}$, $\alpha_i \geq 0$ for $i = 1, 2, 3$. Hence, the condition that the point $\gamma_Z(t)$ belongs to the contact set C^Z if and only if there exists $n \in A(t) \cdot N_Z$ such that $g(x, n, t) = 0$ can be reformulated into the equivalent condition that the point $\gamma_Z(t) \in C^Z$ if and only if $\langle A(t) \cdot N_i, \gamma'_Z(t) \rangle \leq 0$ and $\langle A(t) \cdot N_j, \gamma'_Z(t) \rangle \geq 0$ for some $i, j \in \{1, 2, 3\}$, $i \neq j$. Define functions $q_i : I \to \mathbb{R}$ as $q_i(t) = \langle A(t) \cdot N_i, \gamma'_Z(t) \rangle$ for $i = 1, 2, 3$. Clearly, the contact set C^Z corresponds to the set of closed sub-intervals of the sweep interval I where any two of the functions q_i differ in sign. This is illustrated schematically in Figure 8. At the end-points of these sub-intervals, either $t \in \{t_0, t_1\}$ (illustrated by points a and f in Figure 8) or one of the functions q_i is zero (illustrated by points b, c, c', d and e in Figure 8). Thus the collection of sub-intervals d_Z of I is easily computed. The parametrization function of course is $\gamma_Z : d_Z \to \mathbb{R}^3$ given by the trajectory of the point Z under h. This finishes the parametrization of C^Z.

6 Adjacencies and topology of C

We now focus on the matching of co-edges for each face of C. We already know that faces of C come from (i) C^E when E is a sharp edge, or (ii) C^F when F is a smooth face. Similarly edges in C come from (i) edges bounding faces of C^E, C^F and (ii) edges coming from C^Z, where Z is a sharp vertex. The matching of co-edges is eased by the following **proximity lemma**. While the global brep structure of C may be very different from that of ∂M, we show that locally they are similar.

Recall the natural correspondence $\pi : C \to \partial M$ from Section 3. We show that the adjacency relations between geometric entities of C are preserved by the correspondence π.

Proposition 17. *The correspondence map $\pi : C \to \partial M$ is continuous.*

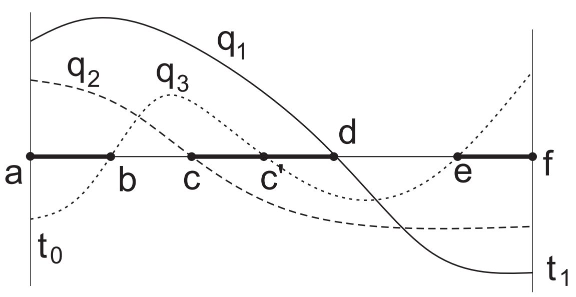

Figure 8: The functions q_1, q_2 and q_3 are plotted against time.

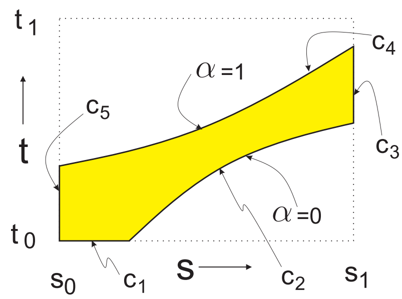

Figure 9: Co-edges bounding face C^E.

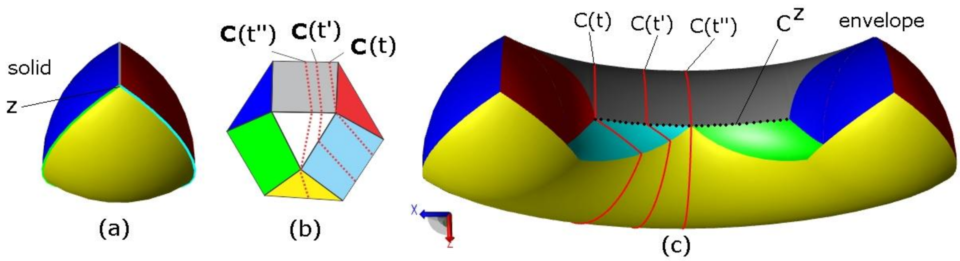

Figure 10: Adjacency relations between faces of C. (a) Solid being swept. (b) Normals of contact $\mathbf{C}(t)$, $\mathbf{C}(t')$ and $\mathbf{C}(t'')$ projected on the unit normal bundle $\mathbf{N}_{\partial\mathbf{M}}$. (c) Curves of contact $C(t)$, $C(t')$ and $C(t'')$ are shown in red. The edge C^Z generated by the sharp vertex $Z \subset \partial M$ is shown as a dotted curve in black on C.

Refer to the appendix for proof.
We conclude the following theorem from the above proposition.

Theorem 18. *For any two geometric entities O and O' of ∂M, if C^O and $C^{O'}$ are adjacent in C, then O and O' are adjacent in ∂M.*

In other words, for a face $F \subset \partial M$ and a sharp edge $E \subset \partial M$, if faces C_i^F and C_j^E are adjacent in C, then F and E are adjacent in ∂M. For a sharp vertex $Z \subset \partial M$, if an edge C_k^Z bounds a face C_j^E in C then the vertex Z bounds the edge E in ∂M.

This aids the computation of adjacency relations amongst entities of C and is illustrated by the sweep example shown in Figures 1, 3 and 12 by color coding. The entities O and C^O are shown in same color.

6.1 Co-edges bounding faces C^E

Consider a sharp edge E supported by smooth faces F and F' in ∂M. We pick a face of C^E given by the component of $\mathcal{F}^E$ shown in Figure 9. The co-edges c_5, c_3 come from the equations $s = s_0$ and $s = s_1$ respectively. These must correspond to edges swept by sharp vertices bounding the edge E. The co-edge c_1 comes from the condition $t = t_0$ and thus comes from curve of contact at the initial time instant and thus, the left cap. Finally, the curves c_2, c_4 correspond to $a_1^E(s,t) = 0$ and $a_2^E(s,t) = 0$ which come from the normals of contact matching that of the supporting smooth faces as described in Section 5. Thus these co-edges must match those coming from the boundaries of C^F and $C^{F'}$.

6.2 Co-edges matching edges of C^Z

We next come to the co-edges matching with edges arising from C^Z. As in Figure 8, the edges of C^Z are parametrized by intervals $d_1, \ldots, d_k$. Each interval d_i has two of the three functions q_1, q_2 and q_3 of one sign and the third of the opposite sign. For example, if we take the interval (c, c'), we see that $q_1, q_3 > 0$ and $q_2 < 0$. For $t \in (c, c')$, if we look at the zero locus of the function $\langle A(t) \cdot n, \gamma_Z'(t) \rangle$, on N_Z, then there must be an $n_1 \in cone(N_1, N_2) \subset N_Z$ such that $\langle A(t) \cdot n_1, \gamma_Z'(t) \rangle = 0$ and there must be an $n_2 \in cone(N_2, N_3) \subset N_Z$ such that $\langle A(t) \cdot n_2, \gamma_Z'(t) \rangle = 0$. This leads us to the sharp edge E_1 with normals N_1, N_2 at the vertex $Z \in E_1$, and to the sharp edge E_2 with normals N_3, N_2 at $Z \in E_2$ and the conclusion that that faces of C^{E_1} and C^{E_2} meet at the edge $[c, c']$ of C^Z. See for example, the curve of contact $C(t')$ in Figure 10(c). A similar conclusion for the interval (c', d) tells us that faces of C^{E_1} and C^{E_3} meet on the edge $[c', d]$ of C^Z. The curious point is the time instant c' where the smooth face F_3 with normal N_3 also meets the edge C^Z. This is illustrated by curve of contact $C(t'')$ in Figure 10(c) where there are four incident faces.

7 Computation of the brep of C

We now explain Steps 14 to 27 of Algorithm 1 for generating the entities on the envelope corresponding to sharp edges and vertices of ∂M. Algorithm 1 marches over each entity O of ∂M and computes the corresponding entity C^O of C. The computation of C^O follows the computation of its boundary ∂C^O. For further discussion fix a sharp edge E of ∂M (cf Step 14 of Algorithm 1).

7.1 Computing and orienting co-edges C^Z

Consider a sharp vertex $Z \subset \partial E$. Recall from Section 5.4 that computing the edges C^Z is equivalent to computing the collection of closed subintervals of the sweep interval I in which the functions q_i differ in sign. We use Newton-Raphson solvers for computing the end-points of these subintervals. Of course, these end-points give rise to vertices which bound edges of C^Z. This is performed in Step 16 of Algorithm 1.

Each co-edge C_i^Z bounding the face C_j^E must be oriented so that C_j^E is on its left side with respect to the outward normal in a right-handed co-ordinate system. Let $y = \gamma_Z(t) \in C_i^Z$ and $\bar{w} \in \mathbb{R}^3$ be tangent to C_i^Z at y. Let n be the outward unit normal to

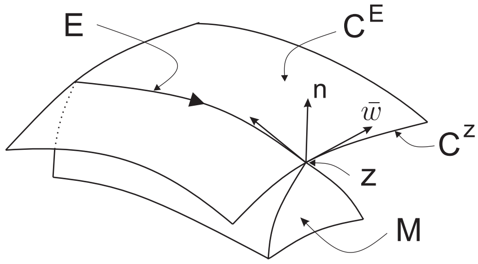

Figure 11: Orienting co-edges C^Z. In this case $e(s_1) = Z$ and $-e'(s)|_{s_1}$ points in the interior of face C^E.

C_j^E at y (cf Section 7.4). Assume without loss of generality that $A(t) = I$ and $b(t) = 0$. Let e be the parametric curve underlying E so that $e(d) = E$ where $d = [s_0, s_1]$. Consider two cases as follows.

1. If $Z = e(s_0)$, then $e'(s_0)$ points in the interior of the face C_j^E, where, e' denotes the derivative of e. If $\langle e'(s_0), n \times \bar{w}\rangle > 0$ then $\bar{w}$ is the orientation of C_i^Z else $-\bar{w}$ is the orientation.
2. If $Z = e(s_1)$ then $-e'(s_1)$ points in the interior of C_j^E. If $\langle -e'(s_1), n \times \bar{w}\rangle > 0$ then $\bar{w}$ is the orientation of C_i^Z else $-\bar{w}$ is the orientation. This is illustrated schematically in Figure 11.

The co-edges C^Z are oriented in Step 17 of Algorithm 1.

7.2 Computing and orienting co-edges $C^E \cap C^F$ and $C^E \cap C^{F'}$

For the sharp edge E supported by smooth faces F and F' in ∂M, the co-edges $C^E \cap C^F$ and $C^E \cap C^{F'}$ bounding a face of C^E correspond to the iso-α curves for $\alpha \in \{0, 1\}$ of C^E as discussed in Section 6.1. The orientation of these co-edges for C^E is opposite to that of the partner co-edges for C^F and $C^{F'}$. The co-edges bounding C^F and $C^{F'}$ are computed and oriented in Steps 6 and 7 of Algorithm 1. Their partner co-edges bounding faces C^E are computed and oriented in Step 20 and 21 of Algorithm 1.

7.3 Computing loops bounding faces C^E

A loop is a closed, connected sequence of oriented co-edges which bound a face. As noted in Section 6.1, the co-edges bounding faces of C^E are either iso-α curves for $\alpha \in \{0, 1\}$, or iso-s curves for $s \in \{s_0, s_1\}$ or iso-t curves for $t \in \{t_0, t_1\}$. In order to compute the loop bounding a face C_i^E, we start with a co-edge bounding C_i^E and find the next co-edge in sequence. For instance, if this co-edge is iso-α curve for $\alpha = 0$ and its end-point is $(\alpha, s) = (0, s_1)$ then the next co-edge in sequence is iso-s curve with $s = s_1$. This is repeated till the loop is closed. Figure 9 illustrates this schematically. This computation is performed in Step 23 of Algorithm 1.

7.4 Computing and orienting faces C^E

The parametrization of faces C^E was discussed in Section 5.2 via the funnel $\mathcal{F}^E$. This is done in Step 24 of Algorithm 1. Each face in the brep format is oriented so that the unit normal to the face points in the exterior of the solid. Consider a point $y = \gamma_z(t) \in C^E$ and assume without loss of generality that $A(t) = I$ and $b(t) = 0$. Recall from Section 5 that if $\bar{w}$ is tangent to E at z, then $n := A(t) \cdot \bar{w} \times \gamma_z'(t)$ is normal to C^E. Further, either $n \in A(t) \cdot N_z$ or $-n \in A(t) \cdot N_z$. Since the interior of the swept volume is $\mathcal{V}^o = \cup_{t \in I} M(t)^o$, the outward normal to C^E at y is n if $n \in A(t) \cdot N_z$ else it is $-n$. This is performed in Step 25 of Algorithm 1.

Our framework is tested on over 100 different solids with number of sharp edges and smooth faces between 4 and 25, swept along complex trajectories. A pilot implementation using the ACIS [18] kernel took between 30 seconds to 2 minutes on a Dual Core 1.8 GHz machine for these examples, some of which appear in Figure 12. Many more examples are included in the supplementary file.

8 Extension to non-simple sweeps

We now discuss the extension of the above framework to 'non-simple' sweeps. Recall that, in a non-simple sweep, the correct construction of the envelope requires an excision of the occluded or the self-intersected part from the contact set. An example of this self-intersection appears in the bottom row of Figure 12. Self-intersections themselves may be classified as *local* or *global* (see [6, 16, 3] for definitions). Global self-intersections are those for which a finite partition of the interval I actually leads to a collection of simple sweeps. The example in Figure 12 is indeed of that type. Global self-intersections are easily resolved by boolean operations on individual simple sweeps and thus needs no new theory. However, local self-intersections are more subtle, where roughly speaking, a point on the contact set is occluded by an infinitesimally close point.

Definition 19. *Given a trajectory h, the* **inverse trajectory** *$\bar{h}$ is defined as the map $\bar{h} : I \to (SO(3), \mathbb{R}^3)$ given by $\bar{h}(t) = (A^t(t), -A^t(t) \cdot b(t))$. Thus, for a fixed point $x \in \mathbb{R}^3$, the inverse trajectory of x is the map $\bar{\gamma}_x : I \to \mathbb{R}^3$ given by $\bar{\gamma}_x(t) = A^t(t) \cdot (x - b(t))$. Observe that, under the trajectory h, the point $\bar{\gamma}_x(t)$ transforms to x at time t.*

The contact set C is said to have a **local self-intersection** (L.S.I.) (see [6, 16]) at a point $y = \gamma_x(t')$ if for all $\delta t > 0$, there exists $t'' \in (t' - \delta t, t' + \delta t)$, such that $\bar{\gamma}_y(t'') \in M^o$, the interior of M. Thus, y is occluded by an infinitesimally close point in the interior of the solid M.

It so happens that all local self-intersections which arise in the general sweep must arise from smooth faces and smooth junctions.

Proposition 20. *For a sharp convex point x on the edge E of ∂M, each point $y = \gamma_x(t')$ lying in the interior of a face of C^E is free of L.S.I.*

Refer to the appendix for proof.

The local self-intersections in the contact set generated by smooth faces of ∂M are analysed in [3], and are already integrated into the framework of Algorithm 1 between steps 10 and 11. This is done by constructing an *invariant* real-valued function θ on the contact set which efficiently separates regions of local and global self-intersections. The function θ is intimately related to

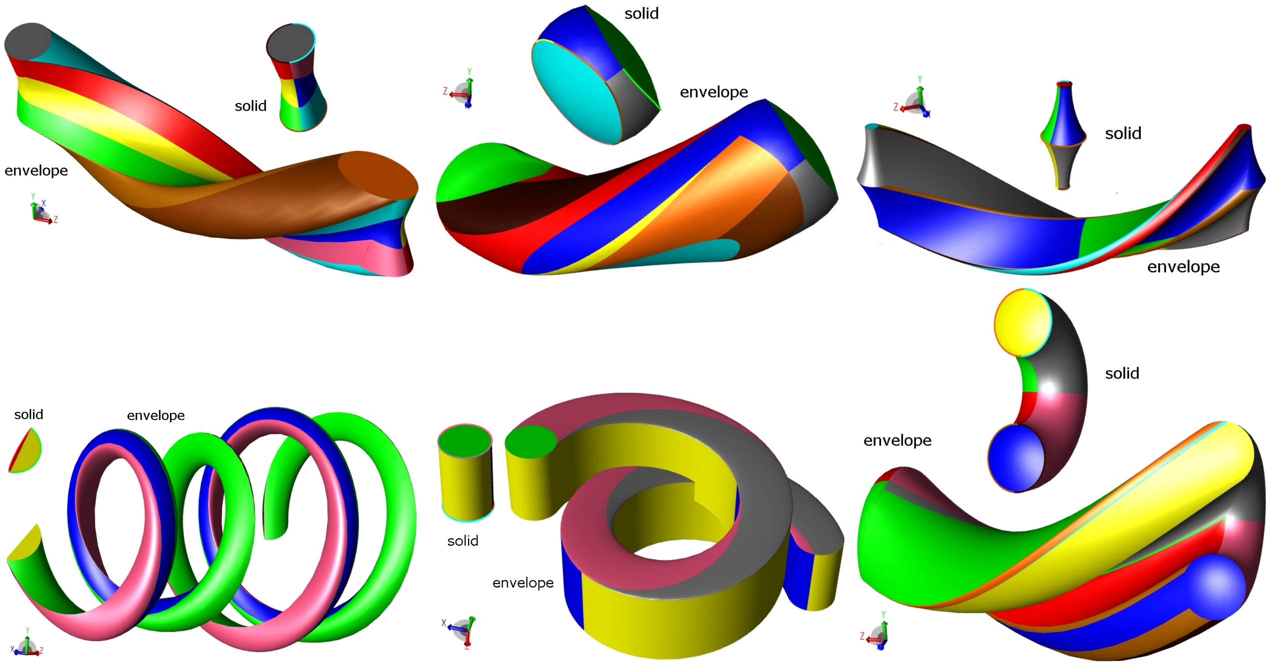

Figure 12: Examples of solid sweep

local curvatures and the inverse trajectory (see [6, 8]) used in earlier works. Further, the 0-level curve of θ identifies all the trim curves of regions with local self-intersection. This provides the 'seed' information for tracing of trim curves. This explains the handling of local self-intersections for all faces of ∂M.

Finally, we come to concave edges (or parts of edges). As there is no outward normal at a concave sharp point, it is easily seen that, in the generic situation, the concave features do not generate any point on the envelope at all. In fact, these will lead to global self-intersections of the contact set and hence result in non-simple sweeps.

9 Conclusion

This paper extends the framework of [4] for the construction of free-form sweeps from smooth solids to solids with sharp features. This was done by developing a calculus of normal cones and their interaction with a one-parameter family of motions. Furthermore, this calculus leads to a neat extension of the key devices of the *prism, funnel* and results in a computationally clean and efficient computation of the trim curves and also of the curves arising from sharp vertices. This in turn leads us to a robust implementation of the general sweep. Numerous models have been successfully generated using this implementation. We have also discussed an extension of the above framework to allow for local and global self-intersections.

The normal bundle indicates a connection between the sweep and the off-set. It is likely that these operations commute, as is indicated by the calculus of cones presented here. Perhaps, this mathematical observation will lead to a better implementation in the future. Finally, the above framework actually constructs the normal bundle of the sweep and that this has several interesting features. For example, it has no sharp vertices (other than those coming from the left or right caps) even though M may have. The sharp vertices of M however lead to degenerate vertices in $\mathcal{E}$.

A Appendix

Proposition 10. *Let $I = [t_0, t_1], t \in I$ and $x \in \partial M$ be such that $\gamma_x(t) \in \mathcal{E}$. Then either (i) $t = t_0$ and there exists $n \in N_x$ such that $g(x, n, t) \leq 0$ or (ii) $t = t_1$ and there exists $n \in N_x$ such that $g(x, n, t) \geq 0$ or (iii) There exists $n \in N_x$ such that $g(x, n, t) = 0$.*

Proof. Define the following subsets of $\mathbb{R}^4$ where the fourth dimension is time. Let $Z := \{(A(t) \cdot x + b(t), t) | x \in M \text{ and } t \in I\}$ and $X := \{(A(t) \cdot x + b(t), t) | x \in \partial M \text{ and } t \in I\}$. Note that Z is a four dimensional topological manifold and X is a three dimensional submanifold of Z. Let $y = \gamma_x(t)$. A point (y, t) lies in Z^o if $t \in I^o$ and $x \in M^o(t)$. If $I = [t_0, t_1]$, the boundary of Z is given by $\partial Z = X \cup (M(t_0), t_0) \cup (M(t_1), t_1)$. Define the projection $\mu : \mathbb{R}^3 \times I \to \mathbb{R}^3$ as $\mu(y, t) = y$. For $z \in Z$ and a point $w \in \mu(z)$, if $\mu^{-1}(w) \cap Z^o \neq \emptyset$ then $w \notin \mathcal{E}$. Hence a necessary condition for w to be in $\mathcal{E}$ is that the line $\mu^{-1}(w)$ should be tangent to ∂Z. For $x \in \cap_{i=1}^m F_i$, the cone of outward normals is $N_x = \{\sum_{i=1}^m \alpha_i \cdot N_i\}$, where $\sum_{i=1}^m \alpha_i = 1$, $\alpha_i \geq 0$ and N_i is the outward normal to face $F_i \subset \partial M$ for $i = 1, \ldots, m$. For $t \in I^o$, the cone of outward normals to ∂Z at the point (y, t) is given by $\mathcal{O} := \{\sum_{i=1}^m \alpha_i \cdot (A(t) \cdot N_i, -g(x, N_i, t))\}$. Further, for $t = t_0$, the cone of outward normals to ∂Z at the point (y, t) is given by $\mathcal{P} := \{\sum_{i=1}^m \delta_i \cdot (A(t) \cdot N_i, -g(x, N_i, t)) - \beta \cdot \hat{e}_4\}$, where $\hat{e}_4 = (0, 0, 0, 1)$ and $\beta, \delta_i \in \mathbb{R}$, $\beta, \delta_i \geq 0$ for $i = 1, \ldots, m$ and $\sum_{i=1}^m \delta_i + \beta = 1$. Similarly, for $t = t_1$, the cone of outward normals to ∂Z at the point (y, t) is given by $\mathcal{Q} := \{\sum_{i=1}^m \delta_i \cdot (A(t) \cdot N_i, -g(x, N_i, t)) + \beta \cdot \hat{e}_4\}$. Consider now case (i). For $t = t_0$, if the line $\mu^{-1}(y)$ is tangent to a point $(y, t_0) \in \partial Z$, then there exists an outward normal to ∂Z in $\mathcal{P}$ which is orthogonal to $\hat{e}_4$, i.e., there exist $\alpha_i \in \mathbb{R}$, $\alpha_i \geq 0$, and $\beta \in \mathbb{R}$, $\beta \geq 0$ such that $\sum_{i=1}^m -\delta_i \cdot g(x, N_i, t_0) = \beta \geq 0$. In other words, there exists $n \in N_x$ such that $g(x, n, t_0) \leq 0$. The proofs for case (ii) and case (iii) are similar. $\square$

Proposition 17. *The correspondence map $\pi : C \to \partial M$ is continuous.*

Proof. For a face $F \subseteq M$, we denote the restriction of the map π to C^F by π^F, i.e., $\pi^F : C^F \to F$, $\pi^F(y) = \pi(y)$. The restriction of π to C^E for a sharp edge $E \subset \partial M$ is defined similarly. Consider first the restriction π^E of π to C^E. Recall the parametrization of C^E via the funnel $\mathcal{F}^E$ and σ^E from Section 5.2. Let $y \in C^E$ and $p = (s', t') \in \mathcal{F}^E$ such that $\sigma^E(p) = y$. The map σ^E being continuous, in order to show that π^E is continuous at y, it is sufficient to show that the composite map $\pi^E \circ \sigma^E : \mathcal{F}^E \to E$ given by $\pi^E \circ \sigma^E(s,t) = e(s)$ is continuous at p, where, e is the parametric curve underlying edge E. This follows from the continuity of e.

The continuity of the restriction π^F to C^F for a face $F \subseteq \partial M$ is similarly proved, by choosing a pair of local coordinates at any point $p \in \mathcal{F}^F$.

The continuity of the map π follows from the fact that π is obtained by gluing the maps $\{\pi^F | F \subseteq M\} \cup \{\pi^E | E$ is a sharp edge in $\partial M\}$ each of which is continuous. □

Proposition 20. *For a sharp convex point x on the edge E of ∂M, each point $y = \gamma_x(t')$ lying in the interior of a face of C^E is free of local self-intersection (L.S.I.).*

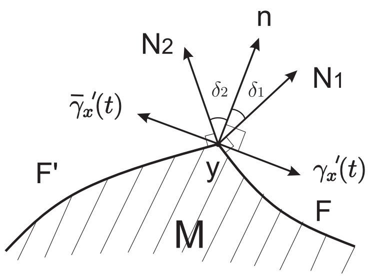

Figure 13: The inverse trajectory is in the exterior of M.

Proof. Let N_x be the cone of unit normals at $x \in E$ formed by N_1 and N_2, where N_1 and N_2 are the unique unit outward normals at x to faces F and F' respectively. Let $n \in N_x$ such that $\langle A(t') \cdot n, \gamma_x'(t')\rangle = 0$. Assume without loss of generality that $A(t') = I$ and $b(t') = 0$. Since y is in the interior of face C^E, $n \neq N_1$ and $n \neq N_2$. Suppose n makes angles $\delta_1 > 0$ and $\delta_2 > 0$ with N_1 and N_2 respectively. Since $\gamma_x'(t') \perp n$, $\gamma_x'(t')$ makes angles δ_1 and $\pi - \delta_2$ with faces F and F' respectively. It is easily verified that $\gamma_x(t') = \bar{\gamma}_x(t')$ and $\gamma_x'(t') = -\bar{\gamma}_x'(t')$, where $\bar{\gamma}_x'(t')$ is the derivative of the inverse trajectory of x. Hence $\bar{\gamma}_x'(t)$ makes angle δ_2 with F' and $\pi - \delta_1$ with F. This is illustrated schematically in Figure 13. The first order Taylor expansion of $\bar{\gamma}_x$ around t' is given by $\bar{\gamma}_x(t' + \delta t) = \bar{\gamma}_x(t') + \delta t \cdot \bar{\gamma}_x'(t')$. Since $\bar{\gamma}_x'(t')$ points in exterior of solid $M(t')$, we conclude that for δt small enough, the inverse trajectory $\bar{\gamma}_x(t)$ is in the exterior of solid $M(t')$ for all $t \in (t' - \delta t, t' + \delta t)$. □

References

[1] K. Abdel-Malek, D. Blackmore, and K. Joy. Swept volumes: Foundations, perspectives and applications. *International Journal of Shape Modeling*, 12(1):87–127, 2006.

[2] K. Abdel-Malek and H.-J. Yeh. Geometric representation of the swept volume using jacobian rank-deficiency conditions. *Computer-Aided Design*, 29(6):457–468, 1997.

[3] B. Adsul, J. Machchhar, and M. Sohoni. Local and global analysis of parametric solid sweeps. *Computer Aided Geometric Design*, 31(6):294–316, 2014.

[4] B. Adsul, J. Machchhar, and M. Sohoni. A computational framework for boundary representation of solid sweeps. *Computer-Aided Design and Applications*, 12(2):181–191, 2015.

[5] D. Blackmore, M. C. Leu, and L. P. Wang. Sweep-envelope differential equation algorithm and its application to nc machining verification. *Computer-Aided Design*, 29(9):629–637, 1997.

[6] D. Blackmore, R. Samulyak, and M. C. Leu. Trimming swept volumes. *Computer-Aided Design*, 31(3):215–223, 1999.

[7] G. Elber. Global error bounds and amelioration of sweep surfaces. *Computer-Aided Design*, 29(6):441–447, 1997.

[8] H. Erdim and H. T. Ilies. Classifying points for sweeping solids. *Computer-Aided Design*, 40(9):987–998, 2008.

[9] H. Ilies and V. Shapiro. The dual of sweep. *Computer-Aided Design*, 31(3):185–201, 1999.

[10] Y. J. Kim, G. Vardhan, M. C. Lin, and D. Manocha. Fast swept volume approximation of complex polyhedral models. *Computer-Aided Design*, 36:1013–1027, 2004.

[11] Kinsley. Timing screw for grouping and turning. https://www.youtube.com/watch?v=LooYoMM5DEo.

[12] S. W. Lee and A. Nestler. Complete swept volume generation, part i: Swept volume of a piecewise c1-continuous cutter at five-axis milling via gauss map. *Computer-Aided Design*, 43(4):427–441, 2011.

[13] S. W. Lee and A. Nestler. Complete swept volume generation, part ii: Nc simulation of self-penetration via comprehensive analysis of envelope profiles. *Computer-Aided Design*, 43(4):442–456, 2011.

[14] R. R. Martin and P. C. Stephenson. Sweeping of three-dimensional objects. *Computer-Aided Design*, 22(4):223–234, 1990.

[15] M. Peternell, H. Pottmann, T. Steiner, and H. Zhao. Swept volumes. *Computer-Aided Design and Applications*, 2:599–608, 2005.

[16] Z. qi Xu, X. zi Ye, Z. yang Chen, Y. Zhang, and S. yuan Zhang. Trimming self-intersections in swept volume solid modelling. *Journal of Zhejiang University Science*, 9(4):470–480, 2008.

[17] J. Rossignac, J. Kim, S. Song, K. Suh, and C. Joung. Boundary of the volume swept by a free-form solid in screw motion. *Computer-Aided Design*, 39:745–755, 2007.

[18] SPATIAL. Acis 3d solid modeling kernel. www.spatial.com/products/3d_acis_modeling.

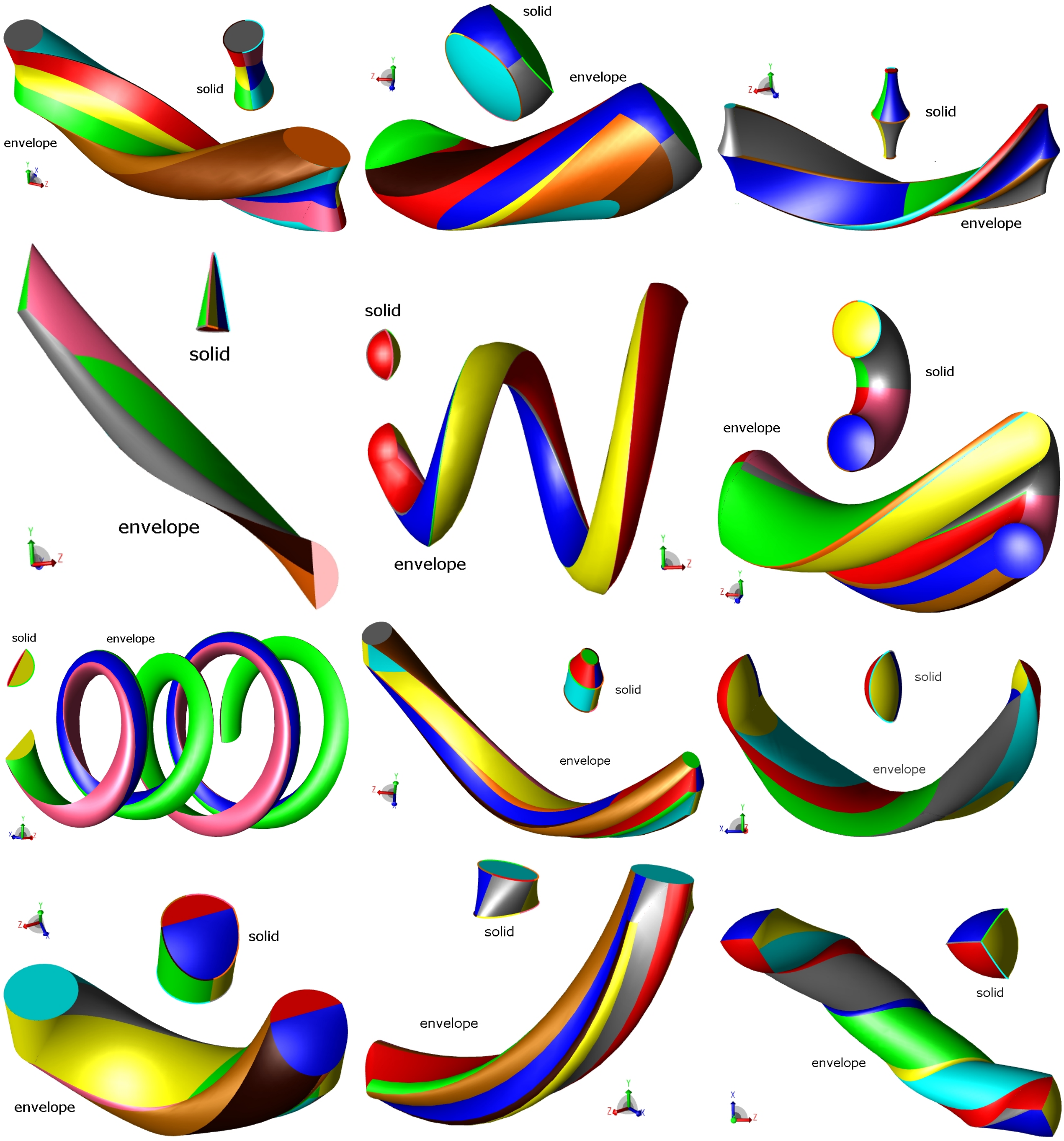

Figure 14: Examples of solid sweep